



## City Research Online

### City, University of London Institutional Repository

---

**Citation:** Zhao, Y., Mehnen, J., Sirikham, A. & Roy, R. (2017). A Novel Defect Depth Measurement Method based on Nonlinear System Identification for Pulsed Thermographic Inspection. *Mechanical Systems and Signal Processing*, 85, pp. 382-395. doi: 10.1016/j.ymssp.2016.08.033

This is the published version of the paper.

This version of the publication may differ from the final published version.

---

**Permanent repository link:** <https://openaccess.city.ac.uk/id/eprint/22034/>

**Link to published version:** <https://doi.org/10.1016/j.ymssp.2016.08.033>

**Copyright:** City Research Online aims to make research outputs of City, University of London available to a wider audience. Copyright and Moral Rights remain with the author(s) and/or copyright holders. URLs from City Research Online may be freely distributed and linked to.

**Reuse:** Copies of full items can be used for personal research or study, educational, or not-for-profit purposes without prior permission or charge. Provided that the authors, title and full bibliographic details are credited, a hyperlink and/or URL is given for the original metadata page and the content is not changed in any way.

---

City Research Online:

<http://openaccess.city.ac.uk/>

[publications@city.ac.uk](mailto:publications@city.ac.uk)

---



# A novel defect depth measurement method based on Nonlinear System Identification for pulsed thermographic inspection



Yifan Zhao\*, Jörn Mehnen, Adisorn Sirikham, Rajkumar Roy

The EPSRC Centre for Innovative Manufacturing in Through-life Engineering Services, Cranfield Manufacturing, Cranfield University, Cranfield MK43 0AL, UK

## ARTICLE INFO

### Article history:

Received 21 June 2016  
Received in revised form  
8 August 2016  
Accepted 22 August 2016  
Available online 30 August 2016

### Keywords:

NDT  
Thermography  
Degradation assessment  
SHM  
Nonlinearity  
Uncertainty

## ABSTRACT

This paper introduces a new method to improve the reliability and confidence level of defect depth measurement based on pulsed thermographic inspection by addressing the over-fitting problem. Different with existing methods using a fixed model structure for all pixels, the proposed method adaptively detects the optimal model structure for each pixel thus targeting to achieve better model fitting while using less model terms. Results from numerical simulations and real experiments suggest that (a) the new method is able to measure defect depth more accurately without a pre-set model structure (error is usually within 1% when  $\text{SNR} > 32 \text{ dB}$ ) in comparison with existing methods, (b) the number of model terms should be 8 for signals with  $\text{SNR} \in [30 \text{ dB}, 40 \text{ dB}]$ , 8–10 for  $\text{SNR} > 40 \text{ dB}$  and 5–8 for  $\text{SNR} < 30 \text{ dB}$ , and (c) a data length with at least 100 data points and 2–3 times of the characteristic time usually produces the best results.

© 2016 The Authors. Published by Elsevier Ltd. This is an open access article under the CC BY license (<http://creativecommons.org/licenses/by/4.0/>).

## 1. Introduction

Over the last decade, pulsed thermography has gained increasing attention due to its rapid, robust, non-contact, non-invasive and in-expensive characteristics. It has been qualitatively and quantitatively applied to different classes of material to detect a variety of in-service degradations [1] such as corrosion in metals, impact damages and delamination in composites [2]. Quantitative characterisation by extracting degradation depth, size, shape and thermal properties has been proven to be effective in pulsed thermography [3–10].

Quantitative prediction of defect depth has been an important research topic over the past 20 years. Most of the proposed methods estimate the defect depth using a characteristic time. For the different methods based on thermal contrast in the normal time scale or logarithmic scale, the peak time of the first or second derivative of temperature curve is usually considered as the characteristic time. The Peak Temperature Contrast method (PTC) [11] calculated the thermal contrast between the defective/damaged region and an adjacent sound or non-defective region. Because of the 3D heat conduction effect, the temperature contrast first increases with time and then decreases [11]. The time at which the temperature difference rises to its maximum value is approximately proportional to the square of the defect depth, and the proportionality coefficient depends on the size of the defect. The smaller the size, the lower the maximum contrast and the

\* Corresponding author.

E-mail address: [yifan.zhao@cranfield.ac.uk](mailto:yifan.zhao@cranfield.ac.uk) (Y. Zhao).

shorter the peak contrast time is [12]. This dependence limits the applications of the PTC method. Peak Slope Time (PST) is corresponding to the peak time of the 1st derivative of thermal contrast. It was found that PST is also approximately proportional to the square of the defect depth and the proportionality coefficient does not depend on the defect size [13]. Krapez et al. [14] proposed to use an early detection of the contrast to recover defect depth that requires a pre-set threshold. Maldague [15] proposed to use the Discrete Fourier Transform (DFT) to calculate defect depth in the frequency domain. It was observed that deeper defects are visible at lower frequencies while shallower defects are detected at higher frequencies. A relationship between the frequency and depth was then studied. All above-mentioned methods require a reference point which is normally chosen from a sound area manually. There are several reports that tried to automatically obtain the reference. Ringermacher et al. [16] used the average temperature from the entire surface before flash as the reference. This works well only when the damaged region is small and the surface is uniformly illuminated. Pilla et al. [17] used the first several frames to calculate a reference temperature. However, sometimes automatic selection of the reference can be challenging, especially when the size of defect is large.

Recently some reference-free methods have been developed. Shepard et al. [18] suggested to use the peak time of the second derivative of temperature decay in the logarithmic scale to determine defect depth, which is also called Log Second Derivative (LSD) method. It is observed that the second derivative peak time  $t_{LSD}$  appears earlier than the Peak Slope Time  $t_{PST}$ , before it is affected by 3D conduction. This method is more accurate than the PST method described above. However, applying the second order differentiation of the temperature can be noisy. A polynomial function fitting of temperature decay was therefore proposed to address this problem, where the second derivative is calculated directly from the fitted model. In this case, fitting the curve on the exact location of the second derivative peak is very important [6]. Zeng et al. [19] proposed an Absolute Peak Slope Time (APST) method to predict the defect depth. A new time-dependent function is obtained by multiplying the original temperature decay with the square root of the corresponding time. The absolute peak slope time  $t_{APST}$  is defined as the peak time of the first derivative of this new function. It has been demonstrated that the square of the defect depth has a linear relation with  $t_{APST}$ . A polynomial model can also be used to fit the new time-dependent function and the first derivative can be calculated directly from the fitted model. All of the methods described are susceptible to signal noise that is typically large in thermography data because the fitted models are data-driven without considering the underlying physics-based models. Sun [6] introduced a method based on Least-Square Fitting (LSF) of a theoretical heat transfer model to the temperature decay for a direct determination of depth. This method also accounts for part of the 3D heat conduction effect and therefore is expected to be more reliable and robust when the 3D effect is significant. Although fitting based on physics-based models, where the model structure is known, reduces the sensitivity to noise, it requires the estimation of multiple unknown parameters simultaneously using optimisation techniques. This can be very time-consuming and requires advanced searching methods.

This paper proposes a Nonlinear System Identification (NSI) method to measure the defect depth in a more automatic and flexible manner. This paper is organised as follows. The proposed method is presented in Section 2. The results and discussions of the numerical simulations and the experimental example are presented in Section 3 while the conclusions are given in Section 4.

## 2. Nonlinear System Identification method

### 2.1. Theory

In pulsed thermographic inspection, the experimental setup of which is illustrated in Fig. 1(a), a short and high energy light pulse is projected onto the sample surface through one or two flash lamps. Heat conduction then takes place from the heated surface to the interior of the sample, leading to a continuous decrease of the surface temperature [6]. An infrared camera controlled by a PC captures the time-dependent response of the sample surface temperature. In areas of the sample surface above a defect (see point 2 in Fig. 1) the transient flow of heat from the surface into the sample bulk is wholly or partially obstructed, thus causing a temperature deviation from the sound areas (see point 1 in Fig. 1). The time when the temperature deviation occurs can be used to estimate the defect depth. The surface temperature due to a defect at depth  $L$  for a plate is given by [20,21].

$$\Delta T(t) = \frac{Q}{\sqrt{\pi\rho ckt}} \left[ 1 + 2 \sum_{n=1}^{\infty} \exp\left(-\frac{n^2 L^2}{\alpha t}\right) \right] \quad (1)$$

where  $\Delta T(t)$  is the temperature variation of the surface at time  $t$ ,  $Q$  is the pulse energy J,  $\rho$  is the material density ( $\text{kg/m}^3$ ),  $c$  is the heat capacity ( $\text{J/K kg}$ ),  $k$  is the thermal conductivity of the material ( $\text{W/(K m)}$ ), and  $\alpha$  is the thermal diffusivity ( $\text{m}^2/\text{s}$ ). In order to obtain a specific characteristic time without a reference curve, Zeng et al. [19,22] proposed to first multiply both sides of Eq. (1) with  $\sqrt{t}$ , and define a new time-dependent function  $f(t)$  as:

$$f(t) = \Delta T(t) \cdot \sqrt{t} = \frac{Q}{e\sqrt{\pi}} \left[ 1 + 2 \sum_{n=1}^{\infty} \exp\left(-\frac{n^2 L^2}{\alpha t}\right) \right] \quad (2)$$

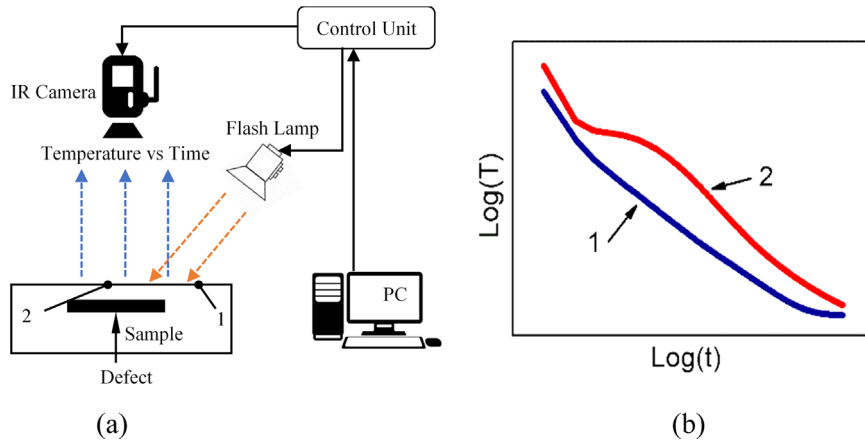


**Fig. 1.** (a) Experimental configuration of the pulsed thermographic inspection, where point 1 denotes a position on the sample surface without defect underneath and point 2 denotes a position with defects underneath; (b) Typical observed time–temperature decay curves in the logarithmic domain for the point 1 and 2, respectively. (For interpretation of the references to colour in this figure legend, the reader is referred to the web version of this article.)

where  $e = \sqrt{\rho ck}$  is the thermal diffusivity. The first derivative of  $f(t)$  is expressed as:

$$f'(t) = \frac{2Q}{e\sqrt{\pi}} \left[ \sum_{n=1}^{\infty} \exp\left(-\frac{n^2 L^2}{\alpha t}\right) \cdot \frac{n^2 L^2}{\alpha t^2} \right] \quad (3)$$

The peak time of  $f'(t)$ ,  $t_{APST}$ , is the corresponding time that the second derivative of  $f(t)$  equals to zero, expressed as

$$f''(t_{APST}) = \frac{2Q}{e\sqrt{\pi}} \left[ \sum_{n=1}^{\infty} \exp\left(-\frac{n^2 L^2}{\alpha t_{APST}}\right) \cdot \frac{n^2 L^2}{\alpha t_{APST}^3} \left(\frac{n^2 L^2}{\alpha t_{APST}} - 2\right) \right] = 0 \quad (4)$$

and the solution can be written as

$$t_{APST} = \frac{L^2}{2\alpha} \quad (5)$$

When multiple reflections are considered, the equation can also be expressed as [19]

$$t_{APST} = \frac{L^2}{1.93\alpha} \quad (6)$$

to provide a more accurate estimation. Eq. (6) is especially suitable for crack detection, where due to the steep slope of crack walls, incident light (from the flash lamp) bounces against the walls several times. Each bounce heats up the crack walls slightly [23], which changes the thermal behaviour slightly in comparison with the single reflection. If  $\alpha$  is known, the value of  $t_{APST}$  can be used to measure the sample thickness or defect depth, or estimate the thermal diffusivity  $\alpha$  if  $L$  is known. In practical applications, thermographic signals are typically corrupted by imaging noise and affected by 3D heat conduction. These uncertainties will be further amplified through calculating the first derivative of  $f(t)$ . Noise therefore affects the accuracy of  $t_{APST}$  measurement and sometimes even no peak is detected. To address this problem, this paper proposes a Nonlinear System Identification (NSI) method to fit  $f(t)$  to improve the fidelity of depth measurement.

## 2.2. Nonlinear System Identification method

Fitting a heat transfer model as shown in Eq. (2) is challenging because in most real-world scenarios too many parameters are unknown. Without considering any physical parameters, a polynomial model can be used to represent the complex thermal behaviour. This can be expressed as

$$f(t) = \sum_{j=0}^N a_j \cdot t^j + \varepsilon(t) \quad (7)$$

where  $N$  is the model order,  $\varepsilon(t)$  is the noise and  $a_j$  are coefficients to be estimated. LSD uses such a model to fit the time–temperature dependency in the logarithmic domain [24]. The challenge is how to automatically select the model order  $N$ . This value should be large enough to ensure a good fit to the observed data. However,  $N$  should also not be too large as it will cause overfitting problems [25]. There is very limited literature to report how to select the model order for fitting time–temperature dependency of active thermographic inspections or discuss about the challenge.

Initially, consider the linear-in-the-parameters model [26]

$$f(t) = \sum_{m=1}^B \theta_m p_m(t) + \epsilon(t) \tag{8}$$

where  $p_m$  are candidate model terms,  $B$  denotes the number of all candidate model terms, and  $\theta_m$  are model coefficients. Let

$$F = [f(1), f(2), \dots, f(M)]^T \tag{9}$$

be a vector of measured data with a total number of  $M$ , and

$$P_m = [p_m(1), p_m(2), \dots, p_m(M)]^T \tag{10}$$

be a vector formed the  $m$ th candidate model term. Let

$$D = \{P_1, P_2, \dots, P_B\} \tag{11}$$

be a dictionary composed of the  $B$  candidate bases. The finite-dimensional set  $D$  is usually redundant. The model term selection problem is equivalent to find a subset

$$D_N = \{\emptyset_1, \emptyset_2, \dots, \emptyset_N\} = \{P_{j_1}, P_{j_2}, \dots, P_{j_N}\} \tag{12}$$

of  $N(N \leq B)$  bases, from the dictionary  $D$ , where  $\emptyset_i = P_{j_i}$ ,  $j_i \in \{1, 2, \dots, N\}$ , so that  $F$  can be satisfactorily approximated using a linear combination of  $\emptyset_m$  as below

$$F = \theta_1 \emptyset_1 + \theta_2 \emptyset_2 + \dots + \theta_N \emptyset_N + \epsilon \tag{13}$$

The first step of the search starts with the initial full model (8) and the initial full dictionary  $D = \{P_1, P_2, \dots, P_B\} = \{1, t, t^2, \dots, t^{B-1}\}$ . Note that the candidate term is not necessary to be  $t^j (j \in \mathbb{Z})$ . It can be any linear or nonlinear relationship, such as  $e^{j \cdot t}$ ,  $\sin(j \cdot t)$ , where  $j \in \mathbb{R}$ . Since the polynomial fitting has been well accepted in this application, the selection of  $D$  is straightforward. For applications where the prior knowledge is limited, some methods have been proposed [27,28], such as bootstrap based structure detection algorithm [29], which is not the research scope of this paper. For  $m = 1, 2, \dots, B$ , let  $q_m = \emptyset_m$  and  $\sigma = F^T F$ , calculate

$$g_m^{(1)} = \frac{F^T q_m}{q_m^T q_m} \tag{14}$$

$$ERR_m^{(1)} = \frac{(g_m^{(1)})^2 q_m^T q_m}{\sigma} \tag{15}$$

Let

$$l_1 = \arg \max_{1 \leq m \leq B} \{ERR_m^{(1)}\} \tag{16}$$

The first significant term can be selected as  $\emptyset_1 = P_{l_1}$ , and the first associated orthogonal vector can be chosen as  $q_1 = P_{l_1}$ . Assume that a subset  $D_{s-1}$ , consisting of  $(s - 1)$  significant terms  $\emptyset_1, \emptyset_2, \dots, \emptyset_{s-1}$ , has been determined at the  $(s - 1)$ th step. In the  $s$ th step, for  $m = 1, 2, \dots, B$  where  $m \notin \{l_1, l_2, \dots, l_{s-1}\}$ , calculate

$$q_m^{(s)} = \emptyset_m - \sum_{r=1}^{s-1} \frac{\emptyset_m^T q_r}{q_r^T q_r} q_r, \emptyset_m \in D - D_{s-1} \tag{17}$$

$$g_m^{(s)} = \frac{F^T q_m^{(s)}}{q_m^{(s)T} q_m^{(s)}} \tag{18}$$

$$ERR_m^{(s)} = \frac{(g_m^{(s)})^2 [q_m^{(s)T} q_m^{(s)}]}{\sigma} \tag{19}$$

Let

$$l_s = \arg \max_{1 \leq m \leq B} \{ERR_m^{(s)}\} \tag{20}$$

The  $s$ th significant terms can then be chosen as  $\emptyset_s = P_{l_s}$ ,  $ERR_m = ERR_m^{(l_s)}$  and the  $s$ th associated orthogonal vector can be chosen as  $q_s = q_{l_s}^{(s)}$ . At each step, the term with the strongest capability to represent the output is selected. The significance of

each selected model term is measured by an index, called the Error Reduction Ratio (ERR), which indicates how much of the variance change in the system response, in percentage terms, can be accounted for by including the relevant model terms. Values of ERR range from 0% to 100%. The larger ERR of a term, the higher the dependence is between this term and the output.

To stop the search procedure and determine the number of significant terms  $N$ , a criteria called Penalised Error-to-Signal Ratio (PESR) is introduced [30]. It can be written as

$$PESR_n = \frac{1}{\left(1 - \frac{\lambda n}{M}\right)^2} \left(1 - \sum_{i=1}^n ERR_i\right) \quad (21)$$

This term was introduced to monitor the search procedure, where  $n$  denotes the index of the selected terms. The search procedure stops when  $PESR_n$  arrives at the first valley. The effect of the adjustable parameter  $\lambda$  on the results is discussed in [30], which suggested that  $\lambda$  should be chosen between 5 and 10. PESR has been used to monitor the search of model structure for various application [31–33].

Once the model structure is determined, the unknown parameters  $\theta_i$  in Eq. (13) can then be estimated using the least square method. The temperature decay curve can be reconstructed by

$$\Delta \hat{T}(t) = \frac{\hat{f}(t)}{\sqrt{t}} = \frac{\theta_1 \varphi_1(t) + \theta_2 \varphi_2(t) + \dots + \theta_N \varphi_N(t)}{\sqrt{t}} \quad (22)$$

The first derivative of  $\hat{f}(t)$  can be calculated by

$$\hat{f}'(t) = \theta_1 \varphi_1'(t) + \theta_2 \varphi_2'(t) + \dots + \theta_N \varphi_N'(t) \quad (23)$$

If  $\alpha$  is known, the thickness can be estimated by

$$\hat{L} = \sqrt{2\alpha \cdot t_{NSI}} \quad (24)$$

where  $t_{NSI}$  denotes the highest peak time of  $\hat{f}'(t)$ . Or if  $L$  is known, the thermal diffusivity can be estimated by

$$\hat{\alpha} = \frac{L^2}{2t_{NSI}} \quad (25)$$

Note the examples of this paper focus on measurement of sample thickness and thermal diffusivity, so the coefficient of 2 was used. To inspect a defective sample, especially when the defect is small, multiple reflections should be considered by replacing the coefficient 2 in Eqs. (24) and (25) with 1.93.

The procedure of the proposed NSI method can be summarised:

- 1) Extract the temperature decay data for a pixel;
- 2) Define a set of candidate terms as shown in Eq. (11). This paper used  $\{1, t, t^2, \dots, t^{B-1}\}$  for all examples;
- 3) Calculate the ERR value of each candidate term, and the term with maximum ERR value is selected;
- 4) Calculate the PESR value after a new term is selected. The term selection procedure stops when PESR arrives the first valley.
- 5) Reconstruct the time–temperature functions  $\Delta \hat{T}(t)$  and  $\hat{f}(t)$  by Eq. (22);
- 6) Calculate the first derivative of  $\hat{f}(t)$  by Eq. (23), and then detect the peak time;
- 7) Estimate the sample thickness or defect depth by Eq. (24) or the thermal diffusivity by Eq. (25);
- 8) Repeat the steps 1–7 for all pixels.

### 3. Results and discussions

#### 3.1. Numerical simulation without noise

To validate the proposed method, numerical simulations were produced by

$$\Delta T(t) = \frac{Q}{e\sqrt{\pi t}} \left[ 1 + 2 \sum_{n=1}^{\infty} R^n \exp\left(-\frac{n^2 L^2}{at}\right) \right] + \varepsilon(t) \quad (26)$$

where the parameters  $Q$ ,  $R$  and  $e$  were set to 1 and the thermal diffusivity was set to  $1 \times 10^{-6}$  m<sup>2</sup>/s. The symbol,  $\varepsilon(t)$ , denotes white noise with a zero mean and a standard deviation  $\sigma_\varepsilon$ . Assume  $\sigma_T$  denotes the standard deviation of the signal without noise. The signal-to-noise ratio (SNR), representing the level of noise, is written as

$$SNR = 20 \log_{10} \frac{\sigma_T}{\sigma_\varepsilon} \tag{27}$$

Initially, simulation data without noise for the thickness value of 2 mm were produced. The proposed NSI method was then applied to these data to estimate the thickness assuming  $\alpha$  is known. The sample rate was chosen as 100 Hz and totally 500 data points (5 s) were sampled. The principle of the proposed method can be demonstrated by Fig. 2 and Table 1. The observed temperature curves  $\Delta T(t)$  and  $f(t)$  are plotted by the solid blue curve in Fig. 2(a) and (b), respectively. The maximum order of the candidate terms  $B$  was chosen as 15. Table 1 shows the values of PESR with different numbers of terms against the selection of the parameter  $\lambda$ . It can be observed that the PESR arrives at the first valley when the number of terms is 9, which is therefore selected as the final number of model terms  $N$ . Furthermore, it is inferred that the selection of  $\lambda$  is not sensitive to the selection of  $N$  due to the fact that  $N$  is chosen as 9 for all considered values of  $\lambda$ . In this paper,  $\lambda$  was chosen as 6 for all examples. The reconstructed  $\Delta T(t)$  and  $f(t)$  can then be produced using Eq. (22), and they are plotted

by the dash red curve in Fig. 2(a) and (b) respectively. Inspection shows that the reconstructed signals fit the observed signals very well, which is also confirmed by inspection of the fitting error between  $f(t)$  and  $\hat{f}(t)$ , shown in Fig. 2(c). The first derivatives of  $\hat{f}(t)$  was then calculated by Eq. (23) and the result is illustrated by Fig. 2(d). The peak of  $\hat{f}'(t)$ , marked by the arrow, was then detected at 2.04 s. If  $\alpha$  is known, the estimated thickness based on Eq. (24) is 2.02 mm. The error is within 1% considering the true value of 2 mm.

To assess the sensitivity of the number of the fitting model order for the LSD and APST methods, Fig. 3(a) compares the estimated thickness using three considered methods (LSD, APST, and NSI) for simulation data without noise against the true thickness. The number of terms was chosen in the range between 5 and 20. Note that the number of terms determines the model order for the LSD and APST methods, which is not the case for the NSI method. It has been observed that, not surprising, for both LSD and APST methods, a higher number of model terms produces better results. It indicates that for data without noise a selection of a high order model of both LSD and APST methods can guarantee an accurate result.

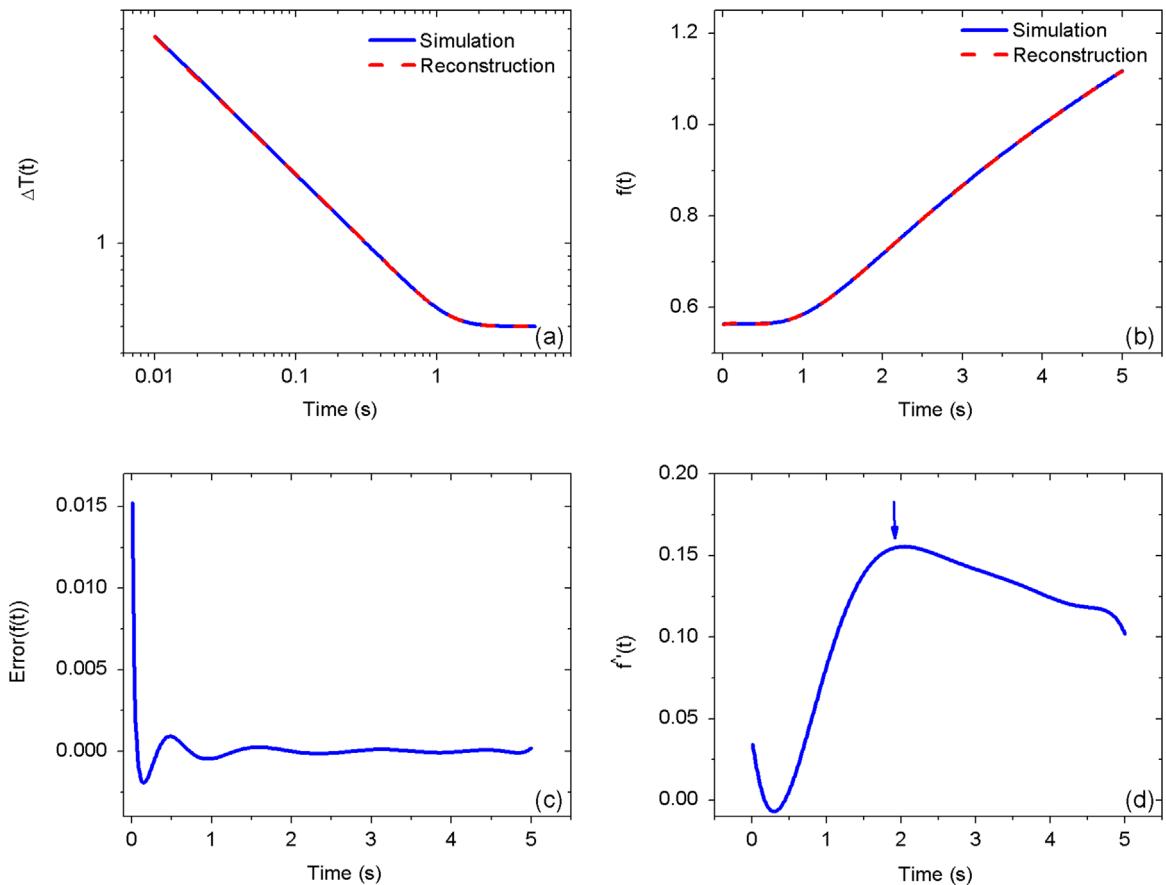


**Fig. 2.** (a) The simulated temperature  $\Delta T(t)$  (blue solid plot) and reconstructed temperature  $\hat{\Delta T}(t)$  (red dash plot) with a thickness of 2 mm, plotted in the logarithmic domain; (b) The simulated  $f(t)$  (blue solid plot) and reconstructed  $\hat{f}(t)$  (red dash plot) temperature curves; (c) The errors between  $f(t)$  and  $\hat{f}(t)$ ; (d) The first derivative of  $\hat{f}(t)$ , where the arrow highlights the peak at the time of 2.04 s. (For interpretation of the references to colour in this figure legend, the reader is referred to the web version of this article.)

**Table 1**

PESR values for different numbers of selected model terms against different values of  $\lambda$ . The final number of model term  $N$  is chosen when the PESR arrives the first valley.

Number of terms	$\lambda$				
	5	6	7	8	9
1	5.132E-01	5.153E-01	5.174E-01	5.195E-01	5.216E-01
2	2.322E-01	2.341E-01	2.361E-01	2.380E-01	2.400E-01
3	2.430E-03	2.460E-03	2.490E-03	2.520E-03	2.560E-03
4	8.770E-04	8.918E-04	9.070E-04	9.226E-04	9.386E-04
5	5.320E-04	5.434E-04	5.551E-04	5.672E-04	5.798E-04
6	8.755E-05	8.983E-05	9.220E-05	9.467E-05	9.723E-05
7	8.284E-05	8.540E-05	8.807E-05	9.087E-05	9.380E-05
8	7.946E-06	8.229E-06	8.529E-06	8.844E-06	9.178E-06
9	<b>2.387E-06</b>	<b>2.484E-06</b>	<b>2.587E-06</b>	<b>2.697E-06</b>	<b>2.814E-06</b>
10	2.390E-06	2.499E-06	2.617E-06	2.743E-06	2.879E-06
11	1.624E-06	1.708E-06	1.798E-06	1.895E-06	2.000E-06
12	3.571E-07	3.774E-07	3.995E-07	4.236E-07	4.499E-07
13	5.997E-07	6.372E-07	6.783E-07	7.236E-07	7.736E-07
14	1.544E-06	1.650E-06	1.767E-06	1.897E-06	2.042E-06
15	2.502E-06	2.688E-06	2.897E-06	3.130E-06	3.392E-06

### 3.2. Numerical simulation with noise

In practice, raw data are contaminated with noise and other signal degradations [11,34]. Errors of temperature measurement with infrared cameras are typically classified into (a) errors of method, calibration errors and electronic path errors [35]. The level of noise is different case to case. To evaluate the performance of all three considered methods against different levels of noise, numerical simulations were produced and analysed with the SNR from 20 dB to 40 dB. For each considered SNR, 100 tests were repeated and the estimated thickness was averaged. Fig. 3(b)–(d) illustrates the results of three examples with the noise level at 40 dB, 30 dB, and 20 dB, respectively. Inspection of these figures clearly indicates that the results for both LSD and APST methods are sensitive to the selection of the model order. The LSD method produced relatively large errors of the estimated thickness when the model order is larger than 14 for the noise level at 40 dB (see Fig. 3(b)), 13 for the noise level at 30 dB (see Fig. 3(c)) and 10 for the noise level at 20 dB (see Fig. 3(d)). Similar results have been observed for the APST method. Determining an optimal number of model order automatically is a challenge because it depends on the level of noise unless the noise level can be determined before applying these methods. This is usually difficult and sometimes impossible for real-world data. It can also be observed that the errors of depth measurement for all considered methods increase following the decrease of SNR. These observations are not surprising because a model with a high order will over-fit the observed signal corrupted by noise. Over-fitting generally occurs when a model is excessively complex, such as having too many parameters relative to the number of observations. The model will describe noise instead of the underlying relationship. This problem can be further amplified during the calculation of the first or second derivative of the model fitting. Fig. 4 aims to explain this problem in more detail. A numerical simulation was produced with a SNR of 20 dB. The mode order was chosen as 13 for both LSD and APST methods. Fig. 4(a) and (c) show the raw  $\Delta T(t)$  and  $f(t)$  with corresponding fitting using LSD and APST, respectively. Fig. 4(b) shows the plot of the second derivative of  $\hat{\Delta T}(t)$  in the logarithmic domain, where the red arrow marks the highest peak selected and the blue arrow marks the peak that should be selected. The over-fitting problem caused an underestimation of the detected thickness, i.e. the detected thickness is 0.22 mm based on Fig. 4(b), which is much smaller than the true value. The plot of the first derivative of  $\hat{f}(t)$  is shown in Fig. 4(d), where the red arrow marks the highest peak and the blue arrow marks the peak that should be selected. The over-fitting problem caused in this case an overestimation, i.e. the detected thickness is 2.18 mm based on Fig. 4(d), which is larger than the true value. However, for the proposed NSI method, the number of model terms is selected automatically by monitoring the trade-off between the model complexity, fitting error and the number of sampling using Eq. (21). This advantage is especially important to analyse real experimental data where the noise levels are unknown. To further evaluate the performance of the proposed technique, Fig. 5 shows the histogram of the estimated thickness for different noise levels. With a decrease of SNR to 20 dB it has been observed that both accuracy and precision, described by the mean and standard deviation respectively, are reduced by inspecting that  $\hat{L}=2.02 \pm 0.02$  mm for 40 dB,  $\hat{L}=2.07 \pm 0.13$  mm for 30 dB, and  $\hat{L}=2.30 \pm 0.32$  mm for 20 dB.

To further explore the results using the proposed method in higher resolution, Fig. 6 shows the averaged values of the selected  $N$  and estimated thickness against the value of SNR as well as corresponding standard derivatives. Fig. 6(a) shows that the value of  $N$  was set to 8 for signals with SNR in the range from 45 dB to 30 dB. For signals with SNR larger than 45 dB, a higher number of  $N$  ( $N > 8$ ) was chosen. For signals with SNR smaller than 30 dB, a relative small number of  $N$  ( $5 \leq N \leq 8$ ) was chosen to avoid the over-fitting problem.

Inspection of Fig. 6(b) shows that for signals with SNR larger than 32 dB, the error of the estimated thickness is within 0.02 mm. For signals with SNR smaller than 32 dB, the error increases almost exponentially following the decrease of SNR

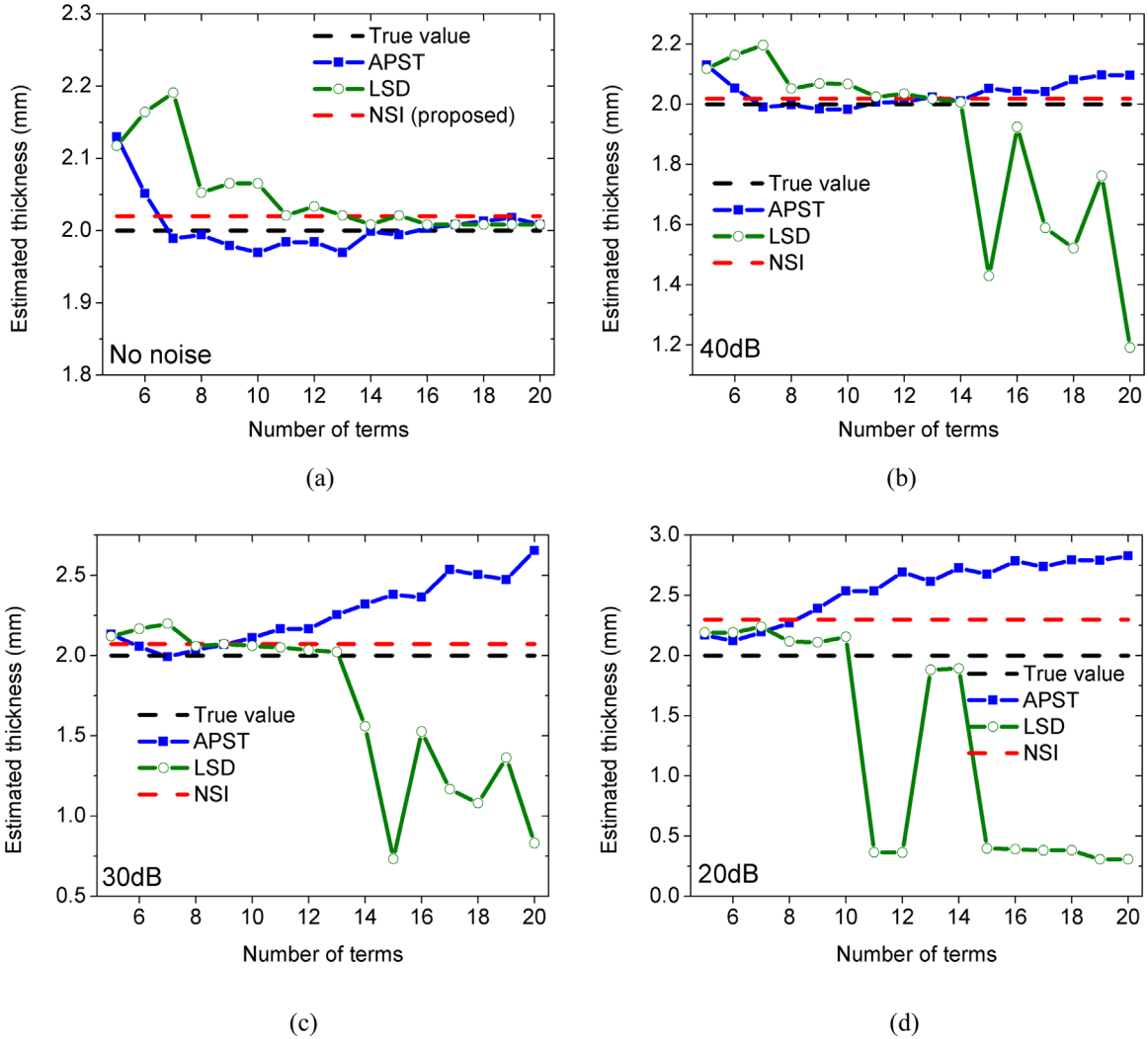


**Fig. 3.** Comparison of estimated thickness using the APST method (the blue plot), the LSD method (the green plot) and the propose NSI method (the red dash line) as well as the true thickness (the black dash line). For the APST and LSD methods, different model orders, from 5 to 20, were tested. For the proposed NSI method, the number of model terms is automatically chosen. This process was applied to numerical simulations data with different levels of noise: (a) no noise, (b) SNR=40 dB, (c) SNR=30 dB, and (d) SNR=20 dB. The results were produced by averaging 100 tests for each considered SNR. (For interpretation of the references to colour in this figure legend, the reader is referred to the web version of this article.)

(increase of noise level), which is mainly due to finding the wrong peak as shown in Fig. 4. The precision of thickness measurement, described by the standard deviation, has the similar trend as the accuracy.

### 3.3. Selection of sampling parameters

This section discusses how the selection of sampling parameters affects the results. Assume that the sampled data length is expressed as  $M_t$  in the unit of time and  $M_p$  is the amount of data point. Obviously,

$$M_p = M_t \cdot f \tag{28}$$

where  $f$  is the sample rate. Let

$$M_t = k \cdot t_{NSI} = k \frac{L^2}{2\alpha} \tag{29}$$

Obviously, to ensure the peak time of  $\hat{f}'(t)$  is detectable, the coefficient  $k$  must be larger than 1. Fig. 7 shows the estimated thickness with different values of  $k$  where  $M_p$  was fixed as 500 to ensure sufficient data for sampling. It has been observed that if  $k$  is between 1 and 1.5 the error of estimation can be up to 0.5 mm due to insufficient sampling. If  $k$  is between 1.5 and 10, the error can be up to 0.2 mm, which is within a more acceptable range. If  $k$  is more than 10, the error is

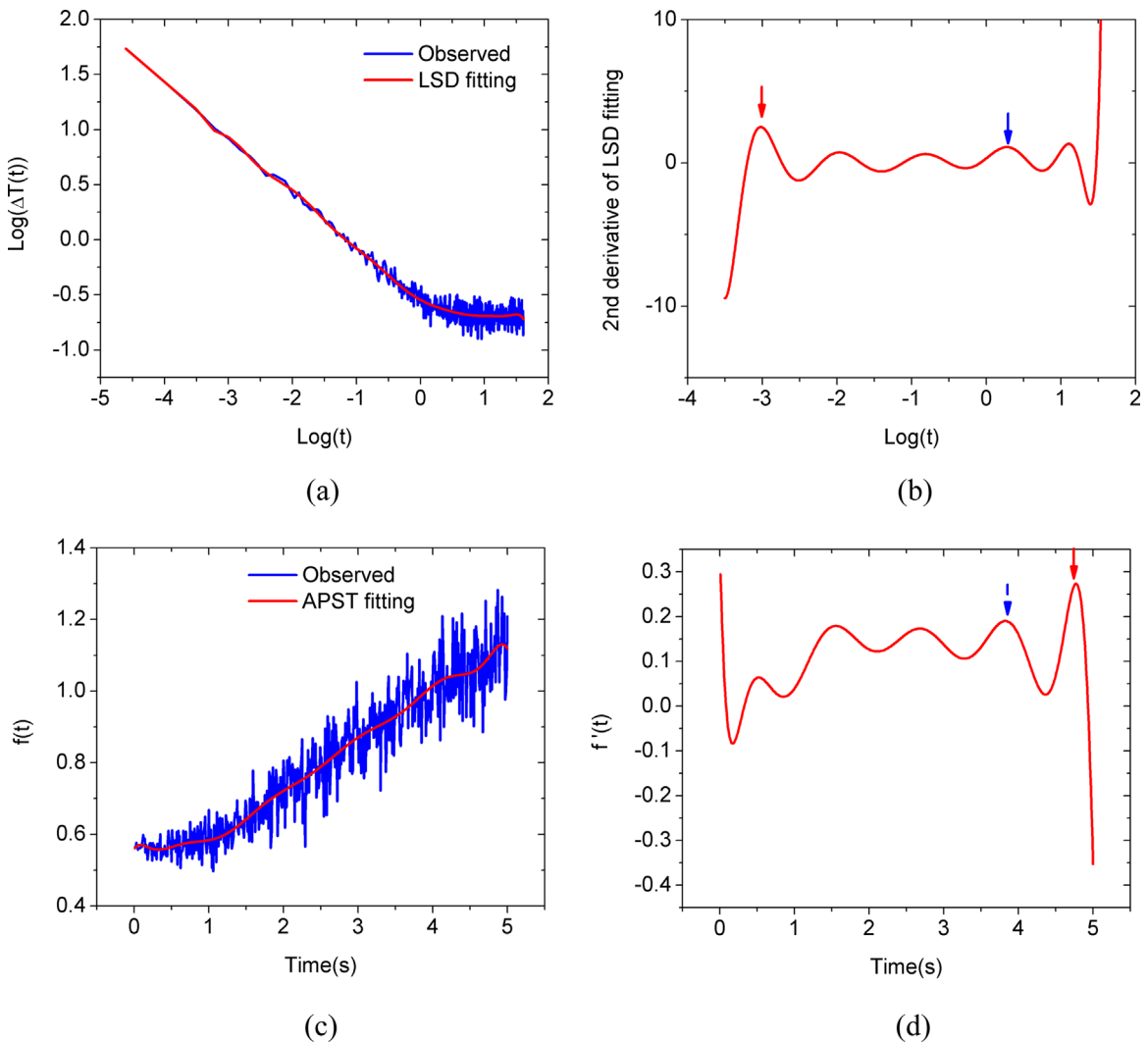


**Fig. 4.** An example of the over-fitting problem where the SNR of the numerical simulation is 20 dB, and the model order was chosen as 13 for both LSD and APST methods. (a): The simulated temperature  $\Delta T(t)$  (the blue plot) and reconstructed temperature  $\hat{\Delta T}(t)$  (the red plot) using the LSD method plotted in logarithmic domain; (b) the second derivative of the LSD fitting where the red arrow marks the peak actually detected and the blue arrow marks the peak that should be detected; (c) The simulated  $f(t)$  (the blue plot) and reconstructed  $\hat{f}(t)$  (the red plot) using the APST method; (d) the first derivative of the APST fitting where the red arrow marks the peak actually detected and the blue arrow marks the peak that should be detected. (For interpretation of the references to colour in this figure legend, the reader is referred to the web version of this article.)

significantly increased because the model primarily fits the data where the temperature is almost stable while the key segment of rapid temperature decay is fitted badly. It is inferred from these plots that the value of  $k$  is recommended to be chosen between 2 and 3.

To determine the minimum number of data points required to produce reliable results, Fig. 8 shows the effect to the results from different values of  $M_t$  where  $k$  was chosen as 2. It has been observed that the error can be up to more than 0.5 mm when  $M_t$  is between 10 and 20. This observation is another proof of over-fitting where the number of observation is

insufficient with a relatively complex model structure. When  $M_t$  is between 20 and 80, the error is significantly reduced. For example, the error is reduced from 0.3 mm to 0.02 mm at a noise level of 50 dB. If  $M_t$  is larger than 80, the variation of error is relatively small for all three cases. Hence, to ensure the reliability of results produced by the proposed method, at least 100 data points are required if the noise level is lower than 35 dB. More data points are suggested if the noise level is higher. Suggested selections for both parameters should be applicable for other data-driven methods.

#### 3.4. Thermal diffusivity measurement

A real example to use the proposed method to measure thermal diffusivity is presented in this session. A defect-free

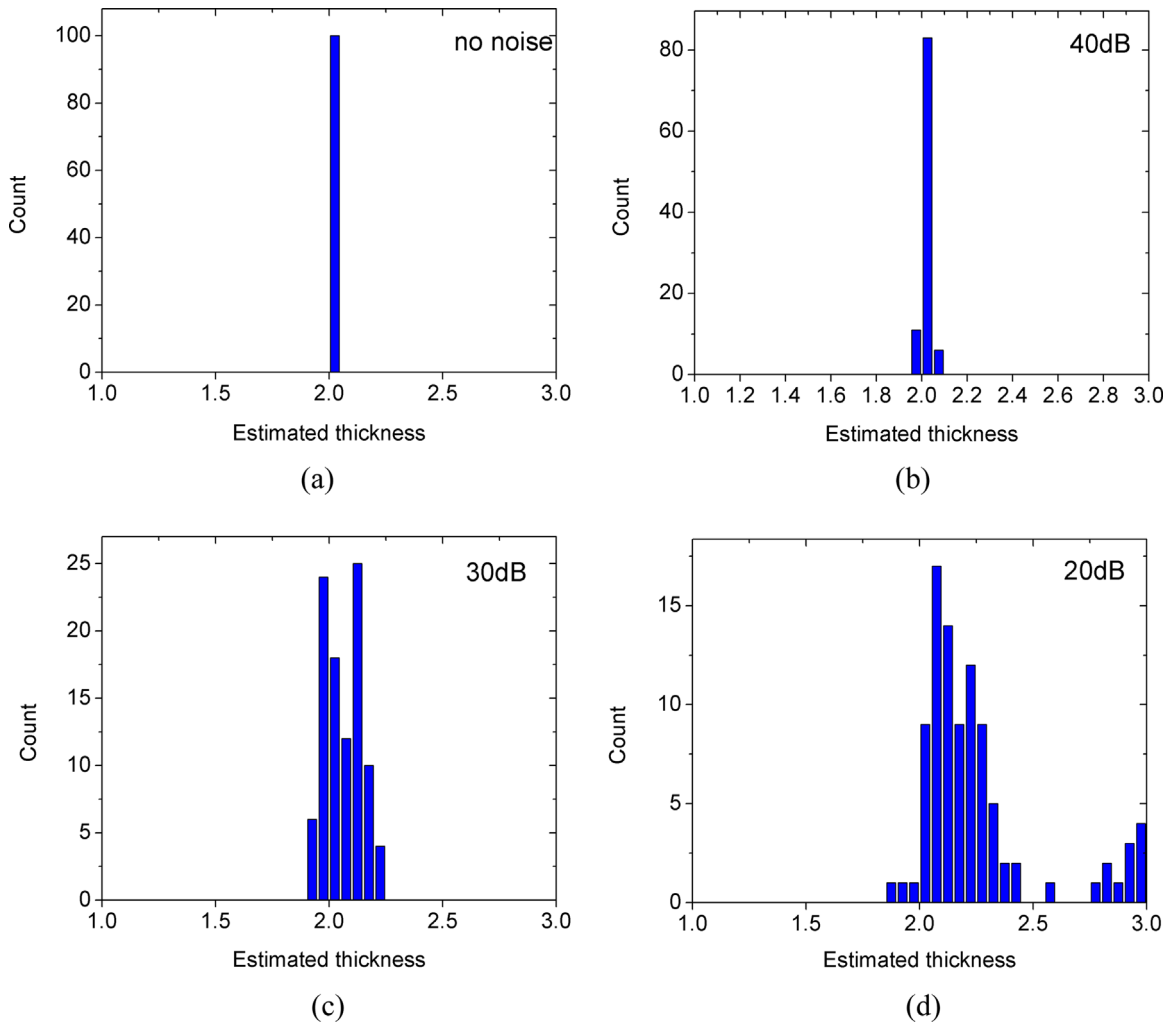


**Fig. 5.** Histogram of the estimated thickness using the proposed NSI method based 100 tests for different levels of noise: (a) no noise, (b) SNR=40 dB (c) SNR=30 dB, and (d) SNR=20 dB. (For interpretation of the references to colour in this figure legend, the reader is referred to the web version of this article.)

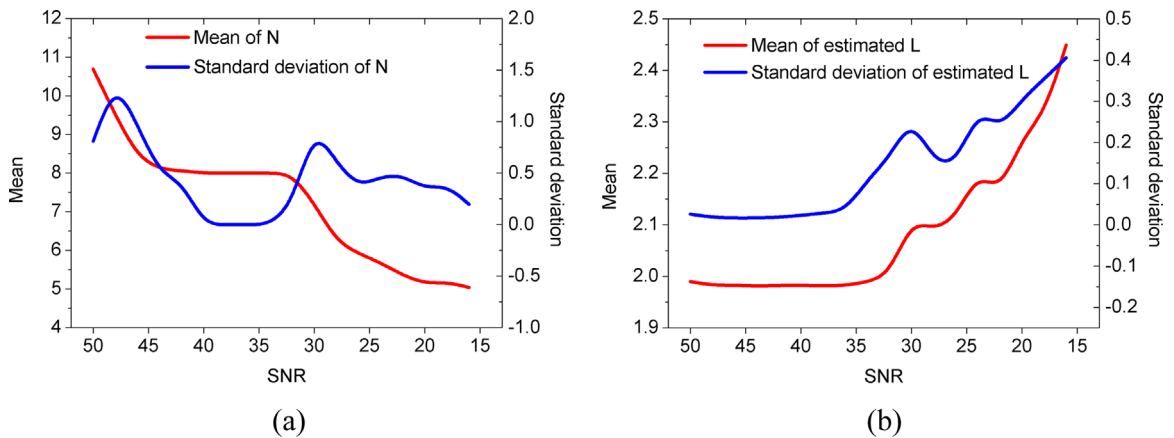


**Fig. 6.** The statistical performance of the proposed NSI method for numerical simulations with different levels of noise. The results were calculated based on 100 tests for each considered SNR. (a) Mean and standard deviation of the selected number of terms against noise level; (b) Mean and standard deviation of the estimated thickness against noise level. (For interpretation of the references to colour in this figure legend, the reader is referred to the web version of this article.)

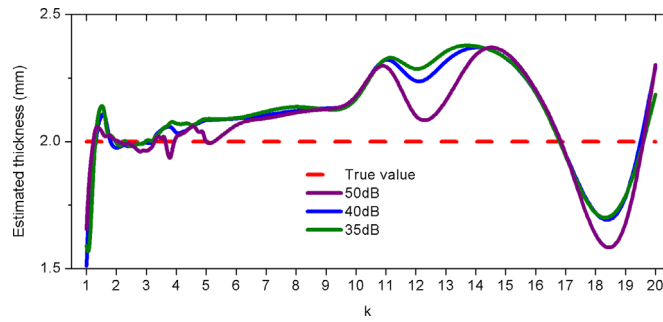


**Fig. 7.** The estimated thickness against the value of ratio  $k$  for the numerical simulations with SNR of 50 dB, 40 dB and 35 dB respectively. (For interpretation of the references to colour in this figure legend, the reader is referred to the web version of this article.)

specimen was produced with the dimension of 150 mm  $\times$  100 mm  $\times$  4 mm, which was made of unidirectional Toray 800 carbon fibres pre-impregnated with Hexcel M21 epoxy resin. The experiment was conducted with the Thermoscope<sup>®</sup> II, a proprietary pulsed-active thermography system from Thermal Wave Imaging Inc. This system comprises of two Xenon flash lamps mounted in an internally reflective hood with a capacitor bank providing power, and a desktop PC to capture and store data. A FLIR SC7000 series infrared radiometer was used, which has an Indium Antimonide (InSb) sensor with a spectral range of 3 – 5.1  $\mu$ m. The radiometer has a full spatial resolution of 640  $\times$  512 pixels. The sample was placed with its surface perpendicular to the camera's line of sight at a distance of 300 mm from the lens. Considering the thickness of the sample and its low thermal diffusivity, a sampling rate of 25Hz was used, and totally 1000 frames, equally 40 s data length, were captured and analysed. More details can be found in [36].

Fig. 9(a) shows the raw temperature  $f(t)$  for three randomly selected pixels from the sample. Note the unit of the y axis is not Celsius but digital intensity outputted by the camera. Similar thermal behaviours for these pixels have been observed.

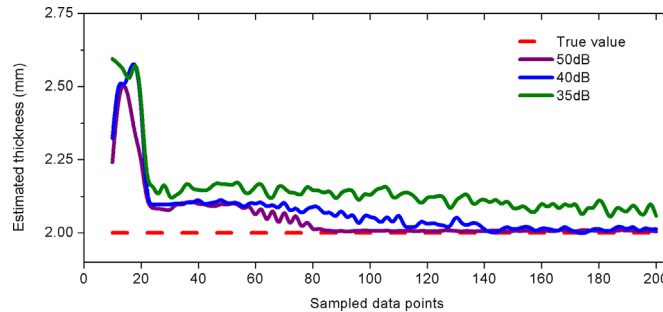


**Fig. 8.** The estimated thickness against the number of sampled data for the numerical simulation with SNR of 50 dB, 40 dB and 35 dB respectively. (For interpretation of the references to colour in this figure legend, the reader is referred to the web version of this article.)

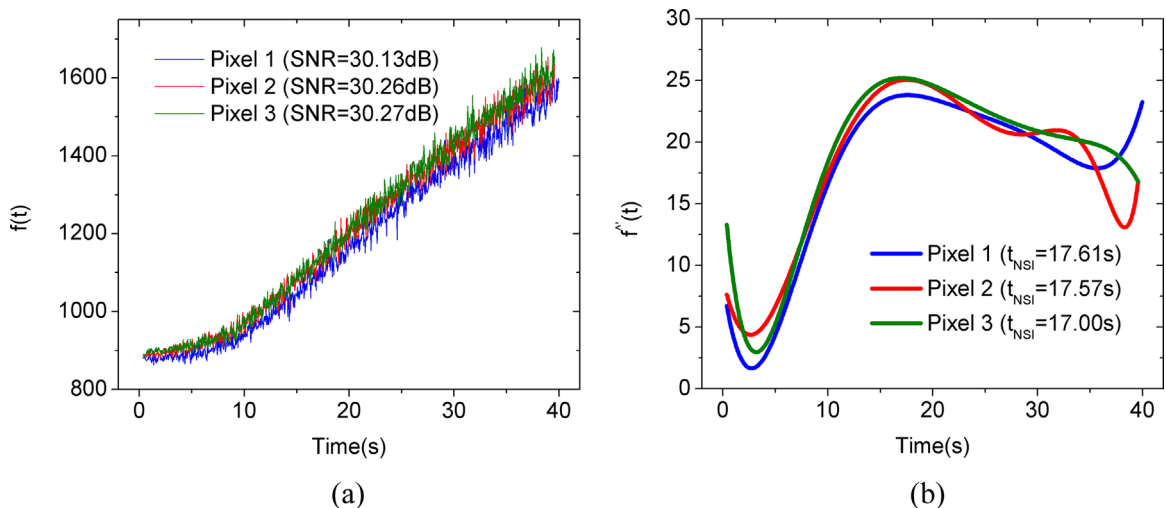


**Fig. 9.** Results for three randomly selected pixels. (a) Raw values of  $f(t)$ ; (b) the first derivative of the reconstructed  $f(t)$ . (For interpretation of the references to colour in this figure legend, the reader is referred to the web version of this article.)

The observed minor difference may be caused by the non-uniform illumination. The value of  $N$  was automatically selected as 8 for all three pixels. Assuming the thermal decay of this experiment follows Eq. (22), the value of SNR for each pixel was calculated and results are 30.13 dB, 30.26 dB, and 30.27 dB respectively. Although the selection of  $N$  was not determined directly by the noise level, the result matches the learned relationship between  $N$  and SNR from numerical simulations, as shown in Fig. 6(a). The plots of the first derivative of the reconstructed  $f(t)$  for three considered pixels after applying the proposed NSI method are illustrated in Fig. 9(b). They exhibit very similar trends from the 5th to 35th second. The peak time,  $t_{NSI}$  was then detected (17.61 s, 17.57 s and 17.00 s respectively) and the thermal diffusivity was calculated by Eq. (25) (0.47 mm<sup>2</sup>/s, 0.47 mm<sup>2</sup>/s and 0.49 mm<sup>2</sup>/s respectively), where  $L$

was assumed to be the same across the specimen. To consider the spatial variation, a region of 100 × 100 pixels, equal to 33 mm × 33 mm, was selected and each pixel inside this region was analysed by the proposed NSI technique and other two methods. Fig. 10(a)–(c) show the thermal diffusivity maps for the selected region from LSD, APST and the proposed method respectively. The result from NSI shows more variations than those from LSD and APST. To evaluate the distribution of the estimated thermal diffusivities, Fig. 10(d)–(e) show the histograms and the corresponding Gaussian fittings for three tested methods respectively. It has been observed that the estimated values are located within a narrow range with an approximate Gaussian distribution. LSD produced a smaller averaged thermal diffusivity (0.41 mm<sup>2</sup>/s) in comparison to those from APST (0.48 mm<sup>2</sup>/s) and NSI (0.47 mm<sup>2</sup>/s). NSI produced the most accurate measurement considering the thermal diffusivity reported by other papers (0.45 mm<sup>2</sup>/s) [37]. LSD fits the curve in the logarithmic domain, which compresses the data of later stage. If the peak time is in the later stage, the accuracy of peak time measurement will be sacrificed due to the compression, which could be the reason why the measured thermal diffusivity from LSD is not as accurate as those from

other two methods. If the peak time is in the early stage, LSD should have no such an issue.

To further explore the results, Fig. 11(a) and (b) show the maps of SNR and the selected  $N$  for the selected region. It can be clearly observed that the bottom side has relatively higher SNR than the top side. The values of  $N$  for most pixels were chosen between 6 and 8.

#### 4. Conclusions

To quantitatively measure defect depth, a polynomial model is normally used in existing methods to fit either the temperature decay in the logarithmic domain or the variation of temperature decay in the time domain. There is very limited literature reporting how the selection of model order affects the results and how to automatically determine the order. A model with a too low order cannot sufficiently fit the observed data, and consequently, depth estimation maybe not

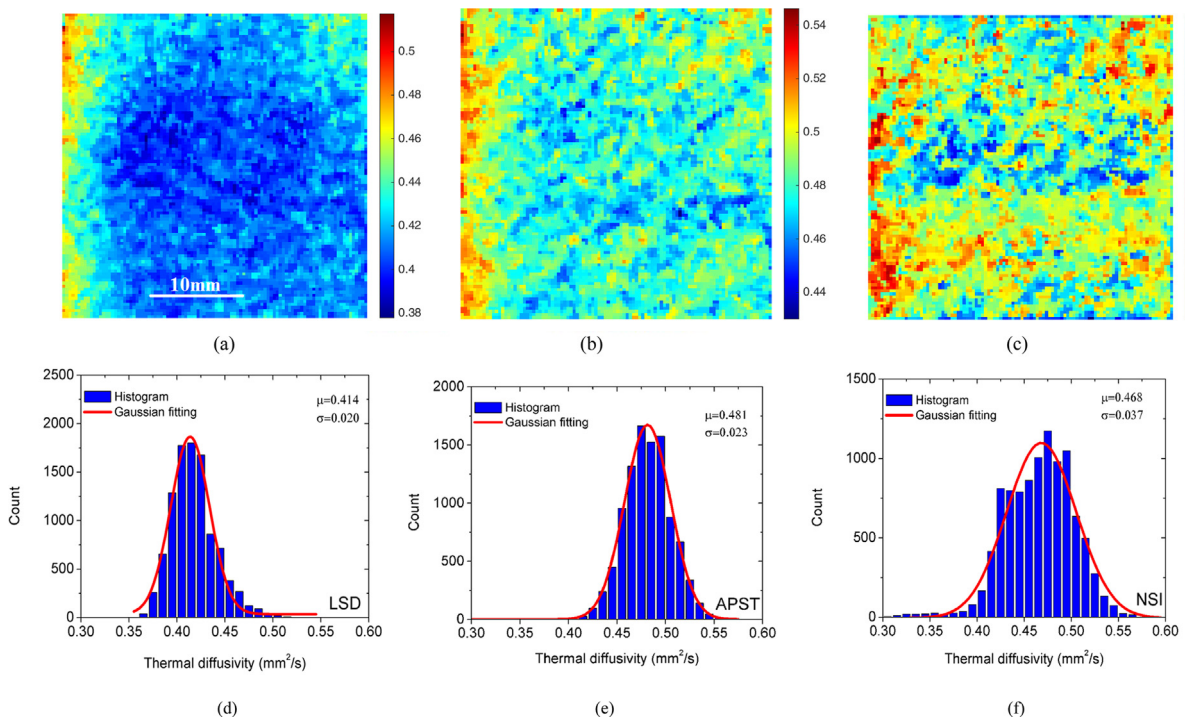


**Fig. 10.** Produced thermal diffusivity map (mm<sup>2</sup>/s) by (a) LSD, (b) APST, (c) the proposed method; histogram of the measurement with corresponding Gaussian fitting from (d) LSD, (e) APST, and (f) the proposed method. (For interpretation of the references to colour in this figure legend, the reader is referred to the web version of this article.)

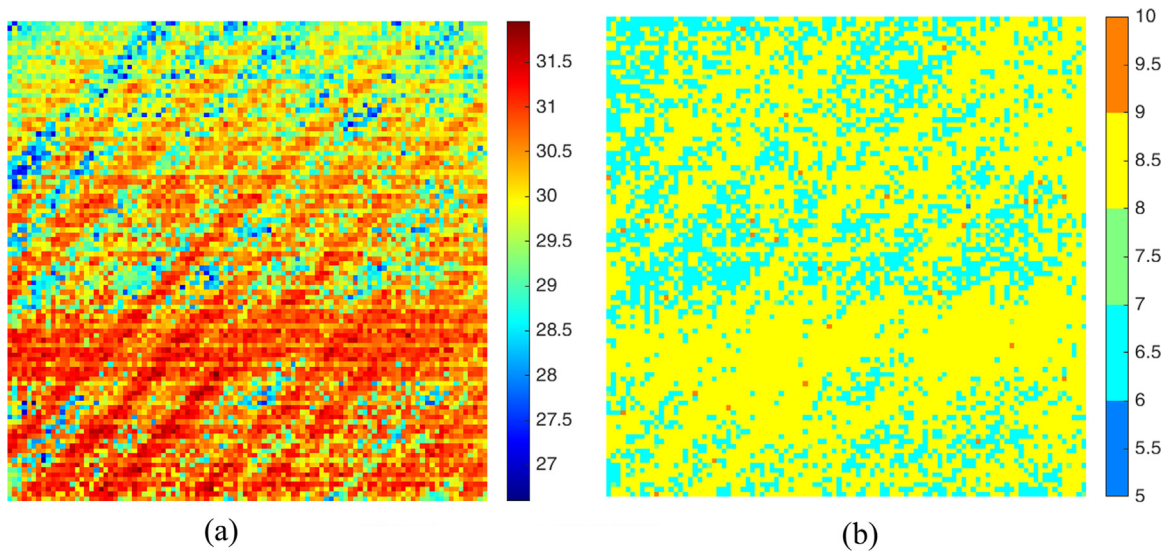


**Fig. 11.** (a) SNR map (dB) measured by the proposed method; (b) the map of the selected  $N$ . (For interpretation of the references to colour in this figure legend, the reader is referred to the web version of this article.)

sufficiently accurate. While a model with a too high order may fit the observed data too well to model the noise rather than the underlying relationship. Such noise will be further amplified when the first or second derivative of fitting is used to measure the depth. These problems have been demonstrated and evaluated in this paper. This is a potential issue towards automation of the pulsed thermographic inspection.

Addressing this problem, this paper has developed a Nonlinear System Identification (NSI) method to model the temperature decay. Different to other methods that build the polynomial model in a one-off manner, the NSI method searches through a relatively large set of candidate model terms to select the most significant model terms one by one. Hence, the model is built in a term-by-term manner. This search will automatically stop when the first valley of the penalised error-to-signal ratio is detected. Furthermore, this method accommodates any linear or nonlinear relationship through the set of candidate terms. The performance of the proposed method including accuracy and precision has been compared with the start-of-the-art depth measurement methods based on numerical simulation with different noise. The impact of the selection of sampling parameters has also been discussed and recommendations have been proposed. The proposed method has been further validated through an experimental example by measuring thermal diffusivity for a composite sample. The results allow the following conclusions:

- The NSI method is able to adaptively detect the model structure for each considered pixel which ensures a better model fitting with relatively less model terms. This characteristic considers spatial variation of the model structure among pixels. Comparing with the LSD and APST methods, this more sophisticated version of model fitting can often measure the depth more accurately while reducing model complexity.
- The number of model terms is determined automatically, which is particularly important for automation of defect/damage depth measurement. Although the numerical simulations in this paper were produced by varying noise levels, in real applications, the noise level is not necessary to be pre-determined because the method itself will evaluate the relationship between the model complexity, fitting error and the number of sampling.
- It has been observed that the number of terms was chosen as about 8 for signals with the SNR in the range from 45 dB to 30 dB. For signals with the SNR larger than 45 dB, a high number of terms (8–10) was chosen. For signals with the SNR smaller than 30 dB, a relative small number of terms (5–8) was chosen. This conclusion should also be applicable to the APST and LSD methods.
- It has been observed from the results of numerical simulations that a sampling data length with twice to three times of  $\frac{L^2}{2\alpha}$  usually produces reliable results. Numerical simulations also show that at least 100 data points are required if the noise level is lower than 35 dB. More data points are suggested if the noise level is higher. These conclusions will aid the practical selection of thermographic parameters such as sampling rate and integration time.

One limitation of the proposed technique is that it is a data-driven method without considering the heat diffusion model underlying the inspection process. Accurate evaluation of noise level is challenging because to achieve this the observed signal has to be clearly divided into 'true signal' and noise. The proposal method can be applied to either measure the thickness of defect-free materials or the defect depth of large defects. Further investigation is required to consider 3D heat conduction for small defects. Another limitation is that the damage is usually assumed to be parallel to the surface, this is

necessary to measure the depth using the NSI technique. Addressing these limitations, further research will focus on reconstructing a 3D representation for defect/damage, degradation volumetric measurement, and determination of the orientation of degradation.

## Acknowledgements

This work was sponsored and supported by the EPSRC Centre for Innovative Manufacturing in Through-life Engineering Services (Grant No: EP/I033246/1). Data underlying this study can be accessed through the Cranfield University repository at <http://dx.doi.org/10.17862/cranfield.rd.3753252?>.

## References

- [1] R. Roy, R. Stark, K. Tracht, S. Takata, M. Mori, Continuous maintenance and the future – Foundations and technological challenges, *CIRP Ann. - Manuf. Technol.* (2016).
- [2] X. Maldague, *Nondestructive Evaluation of Materials by Infrared Thermography*, Springer, New York, 1993.
- [3] J. Mehnert, L. Tinsley, R. Roy, Automated in-service damage identification, *CIRP Ann. - Manuf. Technol.* 63 (1) (2014) 33–36.
- [4] Y. Zhao, J. Mehnert, W. Xu, M. Alrashid, S. Abineri, R. Roy, Degradation assessment of industrial composites using thermography, *Proc. CIRP* 38 (2015) 147–152.
- [5] M.B. Saintry, D.P. Almond, Defect sizing by transient thermography II. A numerical treatment, *J. Phys. D Appl. Phys.* 28 (12) (1995) 2539–2546.
- [6] J.G. Sun, Analysis of pulsed thermography methods for defect depth prediction, *J. Heat Transf.* 128 (4) (2006) 329.
- [7] D.W. Tang, G.H. He, B.L. Zhou, H. Zhang, Effects of finite absorption depth and infrared detector nonlinearity on thermal diffusivity measurement of thin films using the flash method, *Rev. Sci. Instrum.* 66 (8) (1995) 4249.
- [8] W.Y. Jeong, C.J. Earls, W.D. Philpot, A.T. Zehnder, Inverse thermographic characterization of optically unresolvable through cracks in thin metal plates, *Mech. Syst. Signal Process.* 27 (2012) 634–650.
- [9] K. Philipp, A. Filippatos, R. Kuschmierz, A. Langkamp, M. Gude, A. Fischer, J. Czarske, Multi-sensor system for in situ shape monitoring and damage identification of high-speed composite rotors, *Mech. Syst. Signal Process.* 76–77 (2016) 187–200.
- [10] C.J. Earls, Stochastic inverse thermographic characterization of sub-pixel sized through cracks, *Mech. Syst. Signal Process.* 30 (2012) 146–156.
- [11] X.P. Maldague, *Theory and Practice of Infrared Technology for Nondestructive Testing*, Wiley, New York, 2001.
- [12] X. Han, L.D. Favro, P.K. Kuo, R.L. Thomas, Early-Time Pulse-Echo Thermal Wave Imaging in: *Proceedings of the Review of Progress in Quantitative Nondestructive Evaluation*, 1996 MA: Springer US, Boston, 519–524.
- [13] L.D. Favro, X. Han, P.-K. Kuo, R.L. Thomas, Imaging the early time behavior of reflected thermal wave pulses, *Proc. SPIE - Int. Soc. Opt. Eng.* (1995) 162–166.
- [14] J.-C. Krapez, F. Lepoutre, D. Balageas, Early detection of thermal contrast in pulsed stimulated thermography, *J. Phys. IV Colloq.* 04 (C7) . C7-47–C7-50.
- [15] X. Maldague, S. Marinetti, Pulse phase infrared thermography, *J. Appl. Phys.* 79 (5) (1996) 2694.
- [16] H.I. Ringermacher, R.J.A. Jr., W. A. Veronesi, *Nondestructive Testing: Transient Depth Thermography*, US Patent No. 5711603, 1998.
- [17] M. Pilla, M.T. Klein, X.P.V. Maldague, A. Salerno, New Absolute Contrast for Pulsed Thermography, *QIRT 2002 - 6th Int. Conf. Quant. Infrared Thermogr.*, vol. 1, no. 1, pp. 53–58, 2002.
- [18] S.M. Shepard, Reconstruction and enhancement of active thermographic image sequences, *Opt. Eng.* 42 (5) (2003) 1337.
- [19] Z. Zeng, J. Zhou, N. Tao, L. Feng, C. Zhang, Absolute peak slope time based thickness measurement using pulsed thermography, *Infrared Phys. Technol.* 55 (2–3) (2012) 200–204.
- [20] S.K. Lau, D.P. Almond, J.M. Milne, A quantitative analysis of pulsed video thermography, *NDT E Int.* 24 (4) (1991) 195–202.
- [21] C. Maierhofer, P. Myrach, M. Reischel, H. Steinfurth, M. Röllig, M. Kunert, Characterizing damage in CFRP structures using flash thermography in reflection and transmission configurations, *Compos. Part B Eng.* 57 (2014) 35–46.
- [22] Z. Zeng, C. Li, N. Tao, L. Feng, C. Zhang, Depth prediction of non-air interface defect using pulsed thermography, *NDT E Int.* 48 (2012) 39–45.
- [23] F.C. Sham, N. Chen, L. Long, Surface crack detection by flash thermography on concrete surface, *Insight - Non-Destr. Test. Cond. Monit.* 50 (5) (2008) 240–243.
- [24] S.M. Shepard, Temporal noise reduction, compression and analysis of thermographic image data sequences, US 6,516,084 B2, 2003.
- [25] K.Y. Chan, C.K. Kwong, T.S. Dillon, Y.C. Tsim, Reducing overfitting in manufacturing process modeling using a backward elimination based genetic programming, *Appl. Soft Comput.* 11 (2) (2011) 1648–1656.
- [26] S. Chen, S.A. Billings, Representations of non-linear systems: the NARMAX model, *Int. J. Control* 49 (3) (1989) 1013–1032.
- [27] H.L. Wei, S.A. Billings, Model structure selection using an integrated forward orthogonal search algorithm assisted by squared correlation and mutual information, *Int. J. Model. Identif. Control* 3 (4) (2008) 341.
- [28] S.A. Billings, H.L. Wei, An adaptive orthogonal search algorithm for model subset selection and non-linear system identification, *Int. J. Control* 81 (5) (2008) 714–724.
- [29] S.L. Kukreja, H.L. Galiana, R. E. Kearney, Structure detection of NARMAX models using bootstrap methods, in *Proceedings of the 38th IEEE Conference on Decision and Control* (Cat. No.99CH36304), vol. 1, pp. 1071–1076.
- [30] S.A. Billings, H. Wei, Sparse model identification using a forward orthogonal regression algorithm aided by mutual information, *IEEE Trans. Neural Netw.* 18 (1) (2007) 306–310.
- [31] Y. Zhao, H.L. Wei, S.A. Billings, A new adaptive fast cellular automaton neighborhood detection and rule identification algorithm, *IEEE Trans. Syst. Man Cyber. Part B Cyber.* 42 (4) (2012) 1283–1287.
- [32] Y. Zhao, S.A. Billings, H. Wei, F. He, P.G. Sarrigiannis, A new NARX-based granger linear and nonlinear casual influence detection method with applications to EEG data, *J. Neurosci. Methods* 212 (1) (2013) 79–86.
- [33] Y. Zhao, S.A. Billings, H. Wei, P.G. Sarrigiannis, Tracking time-varying causality and directionality of information flow using an error reduction ratio test with applications to electroencephalography data, *Phys. Rev. E* 86 (5) (2012) 051919.
- [34] C. Ibarra-Castaneda, J.-M. Piau, S. Guilbert, N.P. Avdelidis, M. Genest, A. Bendada, X.P.V. Maldague, Comparative study of active thermography techniques for the nondestructive evaluation of honeycomb structures, *Res. Nondestruct. Eval.* 20 (1) (2009) 1–31.
- [35] W. Minkina, S. Dudzik, *Errors of Measurements in Infrared Thermography*, in *Infrared Thermography*, Chichester, UK: John Wiley & Sons, Ltd, pp. 61–80.
- [36] Y. Zhao, L. Tinsley, S. Addepalli, J. Mehnert, R. Roy, A coefficient clustering analysis for damage assessment of composites based on pulsed thermographic inspection, *NDT E Int.* 44 (0) (2016) 59–67.
- [37] C. Meola, G.M. Carlomagno, L. Giorleo, The use of infrared thermography for materials characterization, *J. Mater. Process. Technol.* 155–156 (1–3) (2004) 1132–1137.